Dilution-Triggered SMM Behavior under Zero Field in a Luminescent Zn2Dy2 Tetranuclear Complex Incorporating Carbonato-Bridging Ligands Derived from Atmospheric CO2 Fixation

Manuscript received: 31/05/2013; Article published: 08/08/2013

Dilution-Triggered SMM Behaviour under Zero-Field in a Luminescent Zn_2Dy_2 Tetranuclear Complex Incorporating Carbonato-Bridging Ligands Derived from Atmospheric CO_2 Fixation**

Silvia Titos-Padilla,[1] José Ruiz,[1] Juan Manuel Herrera,[1] Euan K. Brechin,[2] Wolfgang Wersndorfer,[3] Francesc Lloret,[4] and Enrique Colacio[1,]*

[1]Departamento de Química Inorgánica, Facultad de Ciencias, Universidad de Granada. Avda. Fuentenueva s/n, 18071-Granada, Spain.

[2]EaStCHEM, School of Chemistry, Joseph Black Building, University of Edinburgh, West Mains Road, Edinburgh, EH9 3JJ, UK.

[3]Institut Néel-CNRS, Grenoble, 38042, France.

[4]Instituto de Ciencia Molecular (ICMOL), Universitat de València, 46980 Paterna, València, Spain.

[*]Corresponding author; e-mail: ecolacio@ugr.es

[**]Financial support from the Spanish Ministerio de Ciencia e Innovación (MICINN) (Project CTQ-2011-24478), the Junta de Andalucía (FQM-195, the Projects of excellence P08-FQM-03705 P11-FQM-7756), and the University of Granada (Projects GREIB-PYR-2011-13 and Precompetitive Research Projects Programs Ref.-07102011) is acknowledged. S. T.-P. thanks the Junta de Andalucía for a research grant. EKB thanks the EPSRC and Leverhulme Trust for funding. F.L. thanks to the MICINN (Spain) (Project CTQ2010-15364), the University of Valencia (Project UV-INVAE11- 38904) and the Generalitat Valenciana (Spain) (Projects PROMETEO/2009/108, GV/2012/051 and ISIC/2012/002) for financial support. W.W. acknowledges the ERC Advanced Grant MolNanoSpin No 226558. The authors are grateful to A. Molina, CIC, University of Granada, and Dr. A. Rodríguez-Diéguez, Department of Inorganic Chemistry, University of Granada, for their help with magnetic measurements and powder X-ray measurements analysis, respectively.

Supporting information:
Syntheses of the complexes, experimental details, X-ray crystallographic data for 1 and 1′, including data collection, refinement, and selected bond lengths and angles, magnetic data, including dc and ac plots, Cole−Cole plots, and hysteresis plots, and CIF files. This material is available free of charge via the Internet at http://pubs.acs.org

Graphical abstract

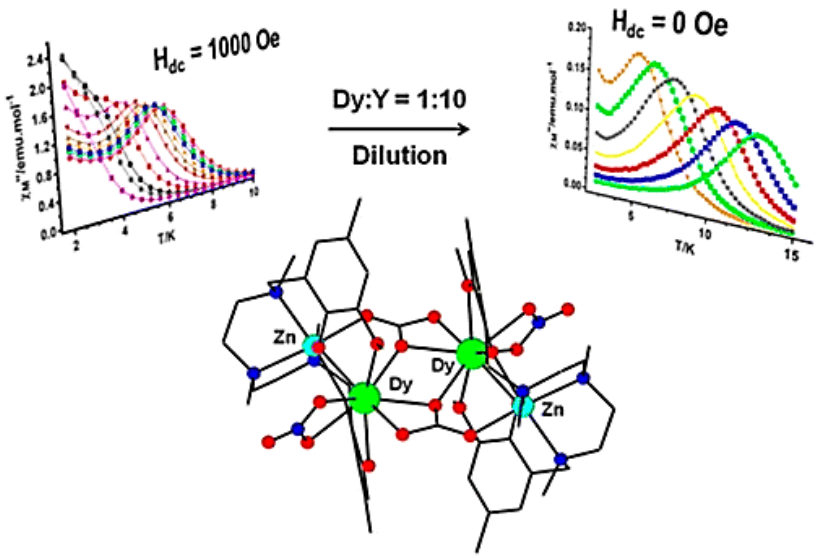

Synopsis

The luminescent tetranuclear complex $\{(\mu_3\text{-}CO_3)\ [Zn(\mu\text{-}L)Dy(NO_3)]_2\}\cdot 4CH_3OH$ does not exhibit SMM at zero applied *dc* field due to a fast quantum tunneling magnetization relaxation process (QTM). However, a 1:10 Dy:Y dilute sample exhibits SMM behaviour at $H_{dc} = 0$ with an important thermal energy barrier $U_{eff} =$ 68 K. The paramagnetic to SMM transformation triggered only by dilution demonstrates the decisive role of the intermolecular dipolar interactions in favoring QTM relaxation.

Abstract

The synthesis structure, magnetic and luminescence properties of the Zn_2Dy_2 tetranuclear complex of formula $\{(\mu_3\text{-}CO_3)_2[Zn(\mu\text{-}L)Dy(NO_3)]_2\}\cdot 4CH_3OH$ **1,** where H_2L is the compartmental ligand N,N',N"-trimethyl-N,N"-bis(2-hydroxy-3-methoxy-5-methylbenzyl)diethylenetriamine, are reported. The carbonate anions that bridge two Zn(μ-L)Dy units come from the atmospheric CO_2 fixation in basic medium. Fast quantum tunneling relaxation of the magnetization (QTM) is very effective in this compound, so that Single-Molecule Magnet behavior is only observed in the presence of an applied dc field of 1000 Oe, which is able to partly suppress the QTM relaxation process. At variance, a 1:10 Dy:Y magnetic diluted sample, namely **1'**, exhibits SMM behavior at zero applied *dc* field with about three-times higher thermal energy barrier than in **1** ($U_{eff} =$ 68 K), thus demonstrating the important role of the intermolecular dipolar interactions in favoring the fast QTM relaxation process. When a dc field of 1000 Oe is applied to **1'**, the QTM is almost fully suppressed, the reversal of the magnetization slightly slows and U_{eff} increases to 78 K. The dilution results combined with

micro-SQUID magnetization measurements clearly indicate that the SMM behavior comes from the single-ion relaxation of the Dy^{3+} ions. The analysis of the relaxation data points out that a Raman relaxation process could significantly affect the Orbach relaxation process reducing the thermal energy barrier U_{eff} for the slow relaxation of the magnetization.

Introduction

The discovery of molecular complexes that can function as single-domain nanoparticles, by exhibiting slow relaxation of the magnetization and magnetic hysteresis below the so-called blocking temperature (T_B), stimulated research activity in the field of the Molecular Magnetism based on coordination compounds. These chemically and physically fascinating nanomagnets, called Single-Molecule Magnets (SMMs),[1-2] straddle the quantum/classical interface showing quantum effects such as quantum tunneling of the magnetization (QTM) and quantum phase interference, and have been suggested for applications in molecular spintronics, ultra-high density magnetic information storage[3] and quantum computing at molecular level.[4] The driving force behind the enormous increase of activity in the field of SMMs is the prospect of integrating them in nano-sized devices.[5] The origin of the SMM behaviour is the existence of an energy barrier (U) that prevents reversal of the molecular magnetization when the field is removed, leading to bistability.[1] Heightened U values can be obtained by increasing the spin multiplicity of the ground state (S_T) or the easy-axis (or Ising-type) magnetic anisotropy of the entire molecule ($D < 0$). Nevertheless, it is very complicated to simultaneously increase both parameters in transition metal clusters as they are interrelated, so that when S_T is very large (observed for high nuclearity clusters), D tends to be low. Consequently, the currently observed energy barriers are low and therefore SMMs act as magnets only at very low temperature. Recently, researchers focused their attention on lanthanide ions (and actinide), as they have large intrinsic magnetic anisotropy and large magnetic moments in the ground state, and therefore could lead to metal complexes with higher energy barriers and improved SMM properties.[6,7] Thus mixed 3d/4f metal aggregates[2,8] and low-nuclearity 4f metal complexes[6,9] have been reported to exhibit slow relaxation of the magnetization with U and T_B values as high as 790 cm^{-1} and 14 K, respectively.[10,11] It should be noted that fast QTM relaxation processes mediated by dipolar interactions, transverse anisotropy or hyperfine interactions can reduce the energy barrier to an effective value (U_{eff}), thus attenuating the SMM properties of the lanthanide-containing species.[1,6] However, in some cases, the exchange coupling between the lanthanide ions, the dilution of the complex within a diamagnetic matrix to eliminate dipolar interactions[12] and the application of a small static magnetic field,[13] to remove the mixing of the ground $\pm Ms$ levels, can partly or fully suppress the QTM relaxation processes enabling the observation of the slow relaxation process through the real thermally activated energy barrier (U).

We,[14] and others,[15] have experimentally shown that the very weak $J_{M\text{-}Ln}$ observed for 3d/4f dinuclear complexes (M^{II} = Cu, Ni and Co) leads to small separations of the low lying split sublevels and consequently to a smaller energy barrier for the magnetization reversal. In view of this, a good strategy to enhance the SMM

properties of the 3d/4f aggregates would be that of eliminating the weak M^{2+}-Ln^{3+} interactions that split the ground sublevels of the Ln^{III} ion by replacing the paramagnetic M^{2+} ions by a diamagnetic ion.[15,16] According to this strategy, we are now pursuing the synthesis of 3d/4f systems in which the paramagnetic M^{2+} ions have been changed by diamagnetic Zn^{2+}.

Herein, we report the synthesis, X-ray structure and detailed dc/ac magnetic susceptibility studies, including dilution and magnetic field dependence, of a $Zn^{II}_2Dy^{III}_2$ tetranuclear complex of $\{(\mu_3\text{-}CO_3)_2[Zn(\mu\text{-}L)Dy(NO_3)]_2\}\cdot 4CH_3OH$ **1**, where H_2L is the compartmental ligand N,N',N"-trimethyl-N,N"-bis(2-hydroxy-3-methoxy-5-methylbenzyl)diethylene triamine (see Figure 1). Compound **1** represents a rare example of lanthanide-containing complex that undergoes a transformation from paramagnetic to high energy barrier SMM under zero-field triggered only by diamagnetic dilution.

Experimental section

Synthetic procedures. The ligand was prepared as previously reported.[14a]

*$\{(\mu_3\text{-}CO_3)_2[Zn(\mu\text{-}L)Dy(NO_3)]_2\}\cdot 4CH_3OH$ (**1**)*. To a solution of H_2L (56 mg, 0.125 mmol) in 5 mL MeOH were subsequently added with continuous stirring 37.2 mg (0.125 mmol) of $Zn(NO_3)_2\cdot 4H_2O$ and 54.8 mg (0.125 mmol) of $Dy(NO_3)_3\cdot 5H_2O$ and 12.6 mg of triethylamine (0.125 mmol). The resulting colorless solution was filtered and allowed to stand at room temperature. After two days, well-formed prismatic crystals of compound **1** were obtained with a yield of 45 % based on Zn. Anal. Calc. for $C_{56}H_{90}N_8O_{24}Zn_2Dy_2$: C, 39.22; H, 5.29; N, 6.54. Found: C, 39.17; H, 5.56; N, 6.74 %. IR(KBr): 3430 (w), 2919 (w), 2863(w), 1538 (s), 1491(s), 1460 (m), 1384 (s), 1352 (m), 1321 (m), 1255 (m), 1070 (w), 848 (w), 812 (w),797 (w).

*$\{(\mu_3\text{-}CO_3)_2[Zn(\mu\text{-}L)Dy_{0.126}Y_{0.874}(NO_3)]_2\}\cdot 4CH_3OH$ (**1'**)***. This diluted complex was prepared by following the same method as for **1** but using 0.0125 mmol of $Dy(NO_3)_3\cdot 5H_2O$ and 0.1125 mmol of $Y(NO_3)_3\cdot 6H_2O$ instead of 0.125 mmol of $Dy(NO_3)_3\cdot 5H_2O$. The colorless crystal of 1' were obtained with a yield of 30% based on Zn. Anal. Calc. for $C_{56}H_{90}N_8O_{24}Zn_2Y_{1.75}Dy_{0.25}$: C, 42.40; H, 5.72; N, 7.06. Found: C, 42.41; H, 5.61; N, 7.44 %. The IR spectrum is virtually identical to that of **1**.

Physical measurements: Elemental analyses were carried out at the "Centro de Instrumentación Científica" (University of Granada) on a Fisons-Carlo Erba analyser model EA 1108. IR spectra on powdered samples were recorded with a Thermo Nicolet IR200FTIR using KBr pellets.

Single-Crystal Structure Determination. Suitable crystals of **1** and **1'** were mounted on a glass fibre and used for data collection on a Bruker AXS APEX CCD area detector equipped with graphite monochromated Mo Kα radiation (λ =0.71073 Å) by applying the ω-scan method. Lorentz-polarization and empirical absorption corrections were

applied. The structure was solved by direct methods using the program SIR-97[17] and SHELXS97[18] and refined with full-matrix least-squares calculations on F^2 using SHELXS97.[18] These programs were used with the package WINGX[19]. The heavy atoms were refined anisotropically. All hydrogen atoms were included at the calculated distances with fixed displacement parameters from their host atoms. The crystallographic data of **1'** refers to one crystal that contains Dy and Y ions in a ratio 0.095/0.905, which are statistically distributed, so that the probabilities of observing ZnDyDyZn, ZnDyYZn and ZnYYZn species are 0.009, 0.172 and 0.82, respectively. We have measured three crystals of the diluted complex **1'** and in all cases the refinements led to Dy/Y ratios of ~ 1/10. Final *R(F)*, *wR(F^2)* and goodness of fit agreement factors, details on the data collection and analysis can be found in Table S1. Selected bond lengths and angles are given in Table S2.

X-Ray powder diffraction analysis. Crystals of **1** were gently ground in an agate mortar and then deposited with care in the hollow of an aluminum holder equipped with a zero back ground plate. Diffraction data (Cu Kα, λ = 1.5418 Å) were collected on a θ:θ Bruker AXS D8 vertical scan diffractometer equipped with primary and secondary Soller slits, a secondary beam curved graphite monochromator, a Na(Tl)I scintillation detector, and pulse height amplifier discrimination. The generator was operated at 40 kV and 40 mA. A scan was performed with $5 < 2\theta < 30°$ with t = 5 seg and $\Delta 2\theta = 0.02°$. LeBail refinement was obtained with the aid of TOPAS-R[20] [triclinic, *P-1* as space group, a = 11.66 Å, b = 12.68 Å, c = 14.16 Å, α = 111.19, β = 104.19, γ = 99.19], verifying the purity of the sample.

Magnetic properties. The variable temperature (2-300 K) magnetic susceptibility measurements on polycrystalline samples of **1** and **1'** under an applied field of 1000 Oe were carried out with a Quantum Design SQUID MPMS XL-5 device. *Ac* susceptibility measurements under different applied static fields were performed using an oscillating *ac* field of 3.5 Oe and *ac* frequencies ranging from 1 to 1500 Hz. *Ac* magnetic susceptibility measurements in the range 1-10000 Hz were carried out with a Quantum Design Physical Property Measurement System (PPMS) using an oscillating *ac* field of 5 Oe. The experimental susceptibilities were corrected for the sample holder and diamagnetism of the constituent atoms by using Pascal's tables. A pellet of the sample cut into very small pieces was placed in the sample holder to prevent any torquing of the microcrystals.

Results and discussion

Complex **1** was prepared from the reaction of H_2L with $Zn(NO_3)_2 \cdot 6H_2O$ and subsequently with $Dy(NO_3)_3 \cdot 5H_2O$ and triethylamine in MeOH by using a 1:1:1:1 molar ratio. Colorless prismatic-shaped crystals of **1** suitable for X-ray analysis, were slowly grown from the solution.

The centrosymmetric tetranuclear structure of **1** (see Figure 1 and Tables S1 and S2 for crystallographic details) consists of two [Zn(μ-L)Dy(NO_3)] dinuclear units connected by two tetradentate carbonate bridging ligands acting with a μ_3–κ^2–O,O' : κ–O : κ–O" coordination mode. The chelating part of the carbonato ligand is coordinated to the Dy^{3+} ion of a dinuclear entity, whereas the remaining oxygen atom is coordinated to the Zn^{2+} ion of the centrosymmetrically related dinuclear unit. Notice that one of the oxygen atoms of the chelating part of each carbonato ligand bridges the two Dy^{3+} ions in a non-symmetric form, giving rise to a rhomboidal $Dy(O)_2Dy$ bridging unit with a Dy-O-Dy bridging angle of 115.72° and two different Dy-O distances of 2.360 and 2.419 Å. The carbonato ligand is presumably generated from the fixation of atmospheric CO_2 in basic medium through the nucleophilic attack of hydroxo species bound to the Ln ions (derived from the deprotonation of coordinated water molecules) to the electrophilic C atom of the CO_2. Similar processes occurring in basic medium have been observed for other carbonate-bridged Dy^{3+} polynuclear complexes.[21,22] The presence of CO_3^{2-} instead of NO_3^- in **1** was proved, apart from charge balance, by IR spectroscopy, as this compound exhibits, compared to the dinuclear one [Zn(H_2O)(μ-L)Dy(NO_3)$_3$]·H_2O (prepared in the same conditions as for **1** but without using triethylamine), a new band at 1538 cm^{-1} assignable to a C-O stretching vibration of the CO_3^{2-} anion (see ESI, figure S1). The same IR band has been observed for other carbonato-bridged Zn-Ln complexes.[23] Powder X-ray measurements were carried out on a polycrystalline sample obtained by grinding a crop of crystals of **1**. The experimental X-ray diffractogram match very well with the theoretical one obtained from the X-ray single crystal structure data (see ESI, Figure S2), thus proving the purity of **1**.

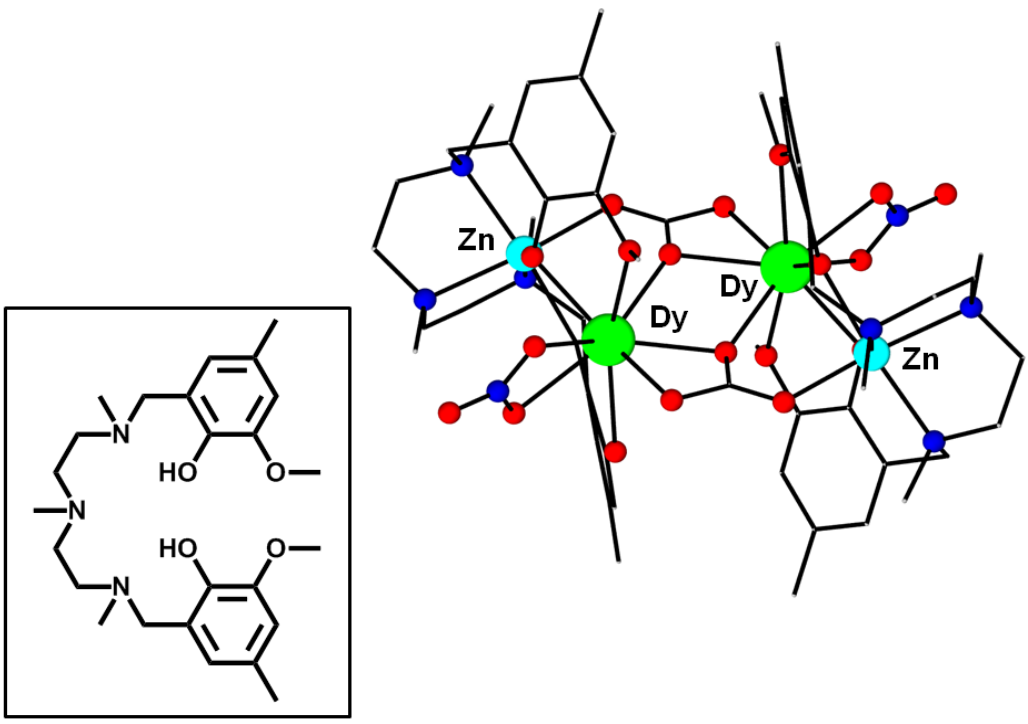

Figure 1. The structure of the ligand H_2L (inset) and a perspective view of the structure of **1**. Colour code: N = blue, O = red, Zn = light blue, Dy = green, C = grey. Hydrogen atoms have been omitted for clarity.

Within each of the [Zn(μ-L)Dy(NO_3)] dinuclear units, Zn^{2+} and Dy^{3+} ions are bridged by two phenoxo groups of the L^{2-} ligand, which wrap around the Zn^{2+} ion in such a way that the three nitrogen atoms from the amine groups, and consequently the three oxygen atoms belonging to the carbonato and phenoxo bridging groups, occupy *fac* positions on the slightly trigonally distorted ZnN_3O_3 coordination polyhedron. The Dy^{3+} ion exhibits a rather non-symmetrical DyO_9 coordination which is made by the two phenoxo bridging oxygen atoms, the two methoxy oxygen atoms, three oxygen atoms from the carbonato bridging groups and two oxygen atoms belonging to a bidentate nitrate anion. This latter and the chelating part of the carbonato ligand occupy cis-positions on the Dy^{3+} coordination sphere. The Dy-O distances are in the range 2.280Å-2.559 Å. In the bridging fragment, the $Dy(O)_2Dy$ and carbonato planes are not coplanar having a dihedral angle of 28.6°. The tetranuclear molecules $\{(\mu_3\text{-}CO_3)_2[Zn(\mu\text{-}LDy(NO_3)]_2\}$ are well separated in the structure by methanol molecules, the shortest Dy···Dy distance being of 12.33 Å. One of the methanol molecules forms bifurcated hydrogen bonds with one of the oxygen atoms of the chelating part of the carbonato ligand and the oxygen atom of the other methanol molecule, with donor-acceptor distances of 2.672 and 2.601 Å, respectively. It should be noted that very recently Tang et al. reported a similar Zn_2Dy_2 tetranuclear complex.[22] The most significant differences between this complex and **1** are: (i) in the former complex, the carbonate bridging fragment is planar, whereas in **1** is not (ii) Dy-O bond distances and the Dy-O-Dy angles in the former complex are, respectively, shorter and larger than those found in **1**. (iii) the Tang's complex has five almost coplanar oxygen atoms around the Dy^{3+} ions, whereas in **1** these five oxygen atoms significantly deviate from the mean plane (iv) complex **1** has a bidentate nitrate ligand coordinated to each Dy^{3+} ion whereas the Tang's complex contains bidentate acetate ligands. The two former points favor a stronger Dy···Dy magnetic exchange interaction through the carbonate bridging groups in the Tang's complex than in **1**, whereas point (iii) favours a larger axial anisotropy in the former.

The direct-current (dc) magnetic susceptibility of **1** has been measured in the 2-300 K temperature range under an applied magnetic field of 0.1 T (Figure S3). The $\chi_M T$ value of 30.15 cm^3 K mol^{-1} at 300 K is compatible with the calculated value of 28.34 cm^3 K mol^{-1} for two non-coupled Dy^{3+} ions ($4f^9$, J =15/2, S = 5/2, L = 5, g = 4/3, $^6H_{15/2}$) in the free-ion approximation. On cooling, the χ_MT product steadily decreases to reach a value of 22.13 cm^3 K mol^{-1} at 2 K. This behavior is due to the depopulation of the Stark sublevels of the dysprosium ion, which arise from the splitting of the $^6H_{15/2}$ ground term by the ligand field rather than from very weak intramolecular interactions between the Dy^{III} ions, as the isostructural Zn_2Gd_2 complex exhibits weak intramolecular ferromagnetic magnetic exchange interaction between the Gd^{3+} ions.[24] For the similar Zn_2Dy_2 complex reported by Tang et al. an increase in χ_MT is observed below 50 K, thus indicating that the Dy···Dy ferromagnetic interaction in this complex is stronger than that found for **1**. The M versus H plot at 2K (right inset Figure S3 inset) shows a relatively rapid increase in the magnetization at low field and then a very slow linear increase to reach a value of 11.54 Nμ_B at the maximum applied field of 5 T. This behavior suggests the presence of a significant magnetic anisotropy and/or more likely the presence of low-lying excited states that are partially [thermally and field-induced] populated. These low-lying excited states

are in agreement with weak magnetic interactions expected for 4f-4f systems. The magnetization value per Dy^{3+} ion at 5 T is considerably smaller than the expected saturation value for one free Dy^{3+} ion of 10 $N\mu_B$ ($Ms/N\mu_B = g_J J = 10$ $N\mu_B$) and is similar to those estimated and observed for other Dy^{III} mononuclear complexes with approximate axial symmetry. This behavior is likely due to crystal-field effects leading to significant magnetic anisotropy, which eliminates the 16-fold degeneracy of the $^6H_{15/2}$ ground state. Notice that the field dependence of the magnetization shows no significant hysteresis above 2 K with the sweep rates used in the SQUID magnetometer.

Dynamic *ac* magnetic susceptibility measurements as a function of the temperature and frequency for **1** are given in Figure 2 and Figure S4, respectively.

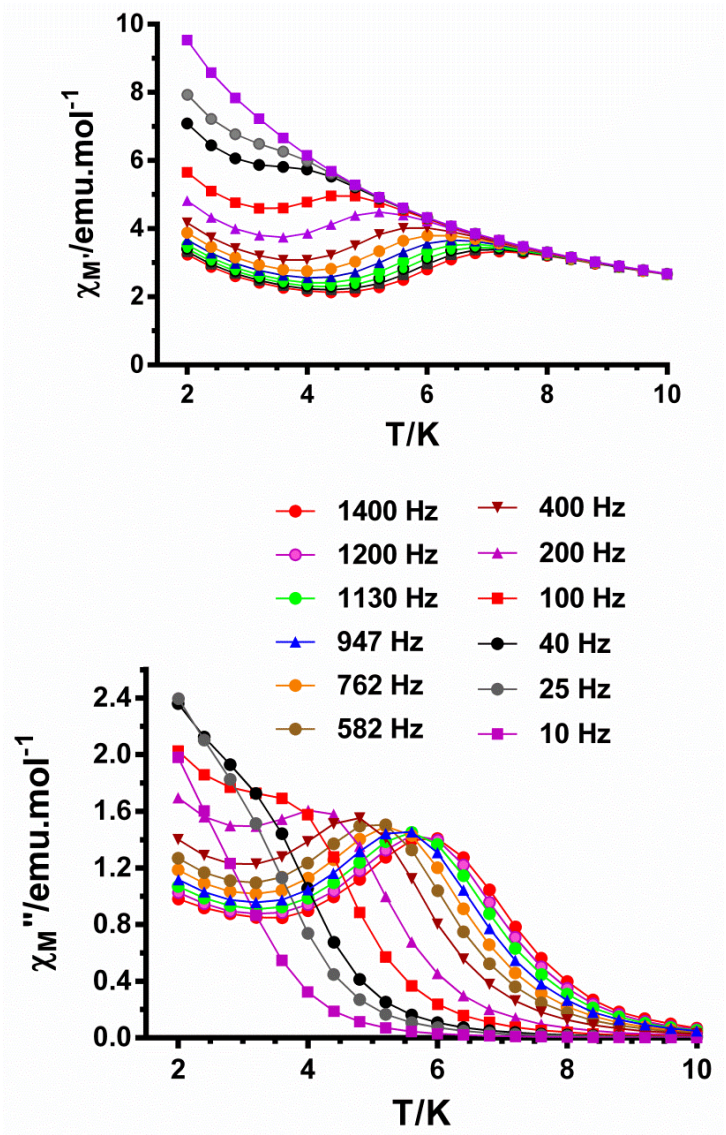

Figure 2. Temperature dependence of the in-phase χ_M' (top) and out-of-pahse χ_M" (bottom) *ac* signals under an applied dc field of 1000 Oe for **1**. Solid lines are guides for the eye.

In spite of the expected large anisotropy of the Dy^{3+} ion, this complex did not show any out-of-phase (χ''_M) signal under zero external field, which can be attributed to the presence of fast relaxation of the magnetization via a QTM mechanism through the thermal energy barrier between degenerate energy levels. As for non-integer spin systems, like Dy^{3+}, transverse anisotropy would not facilitate QTM, this would be mainly mediated by dipole-dipole interactions and/or hyperfine interactions. The similar Zn_2Dy_2 tetranuclear complex reported by Tang et al. shows out-of-phase signals with maxima below 8 K at zero-field and therefore SMM behavior with a $U_{eff} = 34$ K.[22] The suspected larger anisotropy of the Dy^{3+} as well as the stronger Dy···Dy magnetic exchange interaction for this compound compared to **1** may be the reason why slow relaxation of the magnetization is observed at zero-field. In fact, exchange coupling has been found to reduce quantum tunneling of the magnetization at zero applied field.[11]

However, when a small static field of 1000 Oe is applied to fully or partly suppress the quantum tunneling relaxation of the magnetization (this field was chosen because under its application the relaxation process was shown to be the slowest), compound **1** shows slow relaxation of the magnetization as is demonstrated by the appearance below 10 K of out-of-phase peaks in the 3.5(100)-6K (1400 Hz) range. Both χ'_M and χ''_M components (Figure 2) do not go to zero below the maxima at low temperature, which can be taken as a clear indication that the quantum tunneling of magnetization has not been efficiently suppressed.

The Cole-Cole diagram for **1** in the temperature range 4-6 K (Figure S5) exhibits semicircular shapes and can be fitted using the generalized Debye model, affording α values (this parameter determines the width of the distribution of relaxation times, so that $\alpha = 1$ corresponds to an infinitely wide distribution of relaxation times, whereas $\alpha = 0$ represents a relaxation with a single time constant) in the range 0.23-0.06, which suggest the existence of more than one relaxation process operating at low temperatures. The larger α values are associated to the tunneling regime as the QTM relaxation is more susceptible to local strain and/or disorder than the Orbach thermally activated relaxation. The set χ_0 (isothermal susceptibility), χ_S (adiabatic susceptibility) and α obtained in the above fits were further used to fit the frequency dependence of χ_M'' at each temperature to the generalized Debye model, which permits the relaxation time τ to be extracted. The results were then used in constructing the Arrhenius plot shown in the inset of Figure S2. The fit of the data afforded an effective energy barrier for the reversal of the magnetization of 24(1) K with $\tau_o = 2.3 \times 10^{-6}$ s. The Arrhenius plot, constructed from the temperatures and frequencies of the maxima observed for the χ''_M signals in Figure 2, leads virtually to the same result, as expected. In order to know how the intermolecular magnetic dipolar interactions influence the relaxation in compound **1**, we performed *ac* susceptibility measurements on a magnetic diluted sample **1'** (Figures 3 and 4), which was prepared through crystallization with the diamagnetic and isostructural Yttrium complex (see ESI for the crystallographic data) using a Dy/Y molar ratio of 1:10 (the amount of Dy present in the dilute sample was determined to be the 12.6% from the low temperature portions of the *dc* susceptibility for the dilute and the neat compound and is not far from that extracted from X-ray results of 9.5 %). Interestingly, compound **1'** shows slow relaxation of the magnetization

even under zero-field (Figures 3 and 4) with out-of-phase peaks in the 5(100)-13K (10000 Hz) range. The relaxation times were extracted from the fitting of the frequency-dependent *ac* data between 4.5 K and 12.7 K and they follow Arrhenius behavior in the 12.7-8.7 K range with U_{eff} = 68(4) K and τ_o = 9.8 x 10^{-8} s. The Cole-Cole plot (Figure S6) shows in the latter temperature region semicircular shapes with α values in the range 0.04-0.07, thus indicating the presence of a very narrow distribution of slow relaxation in that region. The dramatic increase of the thermal energy barrier in **1'** with regard to **1**, with the concurrent decrease in τ_0, indicates that suppression of intermolecular interactions leads to slower relaxation of the magnetization and SMM behavior at zero-field. The significant U_{eff} thermal energy barrier observed for **1**' is found in high end of the U_{eff} values observed for mono and polynuclear Dy-SMMs.[9]

Even after dilution, a non-negligible fast tunneling relaxation is observed at low temperatures and frequencies at zero-field, as indicated by the divergence in χ''_M below the maxima in the χ''_M *vs* T plot at different frequencies (Figure 4). After applying a small static field of 1000 Oe, which induces the slowest relaxation process, the QTM is almost suppressed (Figure S7 and S8) and the fit of the relaxation times *vs* 1/T data in the 12.7-9.2 K temperature range to the Arrhenius law leads (see Figure 3, top), as expected, to a slight increase of the thermal energy barrier and a decrease of τ_o (U_{eff} = 78(2) and τ_o = 4.7 x 10^{-8} s. In the above temperature region, the α values extracted from the Cole-Cole plot (Figure S9) are in the 0.03-0.08 range, which also supports the presence of a very narrow distribution of slow relaxation in the high temperature region. Nevertheless, the fact that under an applied magnetic field of 1kOe, when the QTM is almost suppressed, the experimental relaxation times deviate from the Orbach linear law in the 4.5-12.7 K temperature region could indicate the presence of multiple relaxation processes. In view of this, we have fitted the experimental data to the following equation that considers that the spin-lattice relaxation takes place through Raman and Orbach processes:[25]

$$\tau^{-1} = BT^n + \tau_0^{-1} \exp\left(-U_{eff}/kT\right)$$

The first and second term correspond to the Raman and Orbach processes, respectively. In general n = 9 for Kramers ions,[25] but depending on the structure of the levels, n values between 1 and 6 can be considered as reasonable.[26] The best fit of the experimental data in the above temperature range afford n = 5.2(3), B = 0.04(2), τ_0 = 2.5x10^{-8} and U_{eff} = 121(4) K (Figure 3 top, red line). These results seem to indicate that the Raman relaxation process significantly affects the Orbach relaxation process reducing the thermal energy barrier U_{eff} for the slow relaxation of the magnetization.

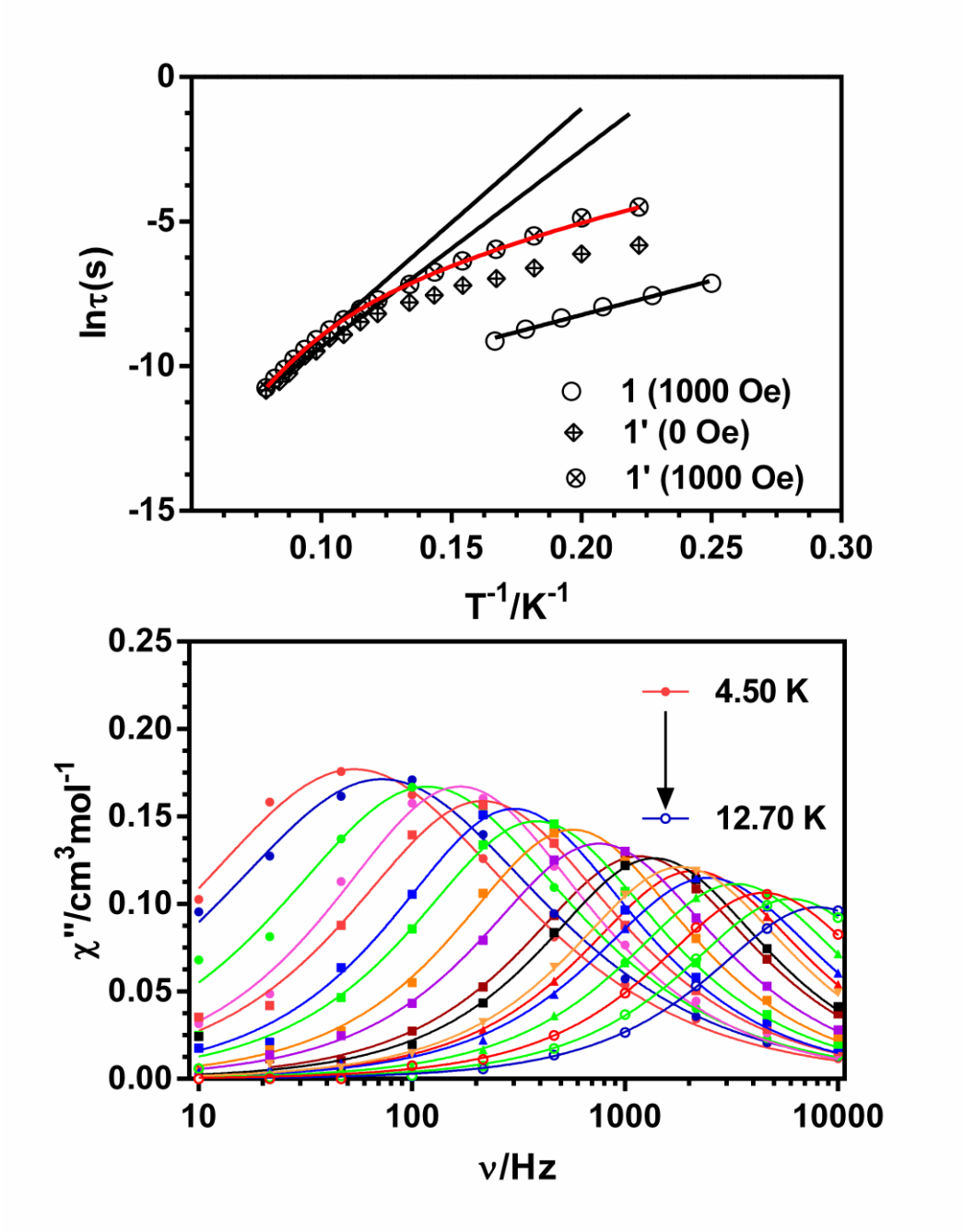

Figure 3. Top: Arrhenius plots of relaxation times of **1** under 1 kOe and **1'** under 0 and 1 kOe. Black solid lines represent the best fitting of the experimental data to the Arrhenius equation. Red line represents the best fit to a Orbach plus Raman relaxation processes. Bottom: Temperature dependence of the molar out-of-phase ac susceptibility (χ_M'') for **1'** under 0 Oe dc applied field. Solid lines represent the best fitting of the experimental data to the Debye model.

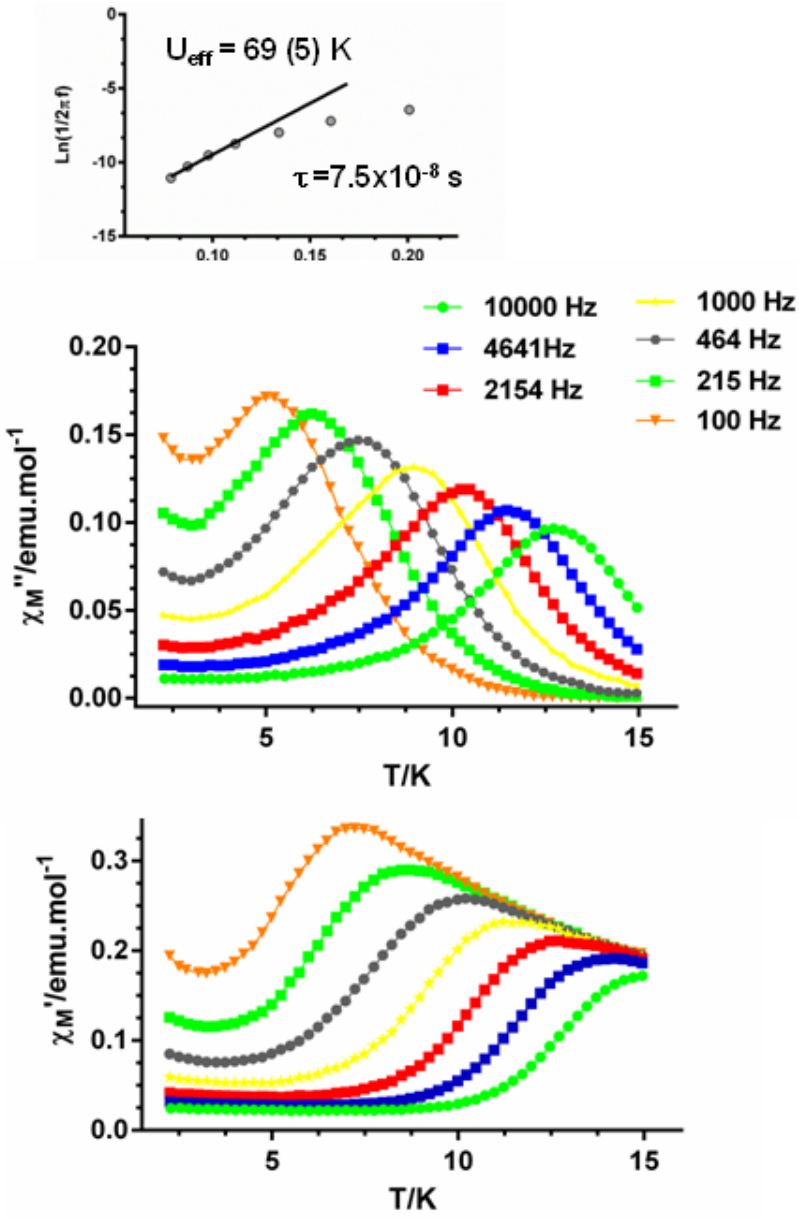

Figure 4. Temperature dependence of the in-phase χ_M' (bottom) and out-of-phase χ_M" (medium) *ac* signals at zero applied dc field for **1'** at different frequencies. Arrhenius plot for **1'** constructed from the temperatures of the maxima and the corresponding frequencies.

We have performed magnetization hysteresis loop measurements in the 0.03-4 K temperature range using a μ-SQUID instrument[27] with the aim of studying the magnetization dynamics and to confirm the SMM properties of **1** and **1'**. Magnetization vs applied dc field hysteresis loops at different temperatures and sweeping rates are given in Figure 5. Hysteresis loops were measured on single-crystals, which were aligned with the easy axis of magnetization using the transverse field method.[28] For **1**, a large step is observed at zero field without hysteresis (Figure 5a), which is consistent with the QTM generally found for 4f containing complexes and with the tail that exhibits this compound at

low temperature in the χ_M" *vs* T plot. When the field is increased, below 1 K, hysteresis loops are observed with a small opening, their coercitivities being temperature and field sweep rates dependent. The maximum opening occurs below 1500 Oe, which agrees well with the *ac* optimum field of 1000 Oe. As expected for SMM, the coercitivity increases with decreasing temperature and increasing field sweep rates. Surprisingly, below 0.5 K, the coercive field decreases with decreasing temperature. This behavior has been observed for other Dy-containing SMMs and ascribed to a reduction of the tunneling due to thermal activations around the tunnel splitting.[29]

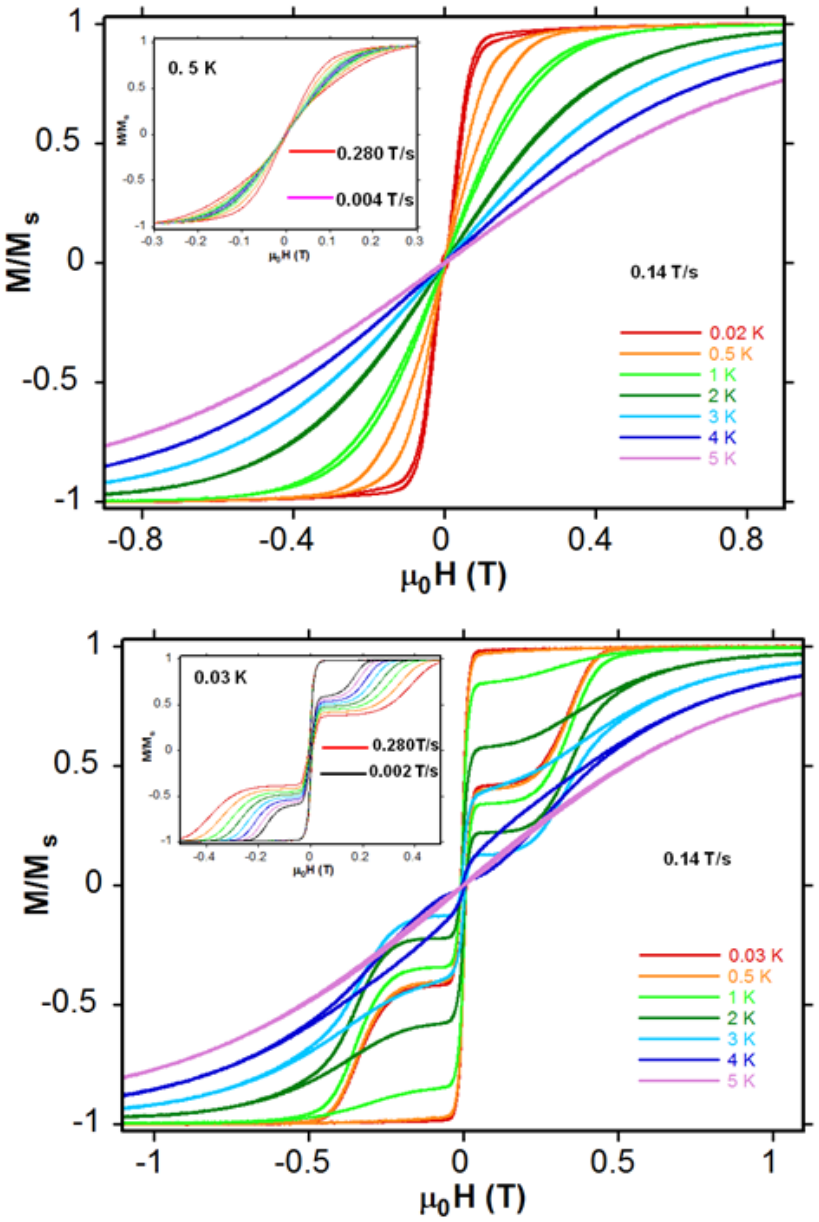

Figure 5. Top: Normalized magnetizations (M/Ms) vs applied dc field sweeps at the indicated sweep rate and temperatures for 1. Inset: Using sweep rates between 0.004T/s and 0.280 T/s at 0.03 K. Bottom: The same plots for 1'.

For the 1:10 diluted complex **1'**, two-step butterfly shaped hysteresis loops were observed below 4 K (Figure 5b), whose coercitivity, as expected, increases with decreasing temperature and increasing field sweep rates. The fact that there exists significant coercive field at zero field for **1'** demonstrates: (i) the magnetic site doping can significantly suppress the QTM and (ii) the hysteresis is essentially a single-ion feature rather than due to a long-range ordering or magnetic interactions. In fact for a 1:10 Dy:Y diluted system the probability for observing the dinuclear species ZnDyYZn is 0.18 whereas that of the ZnDyDyZn species is only 0.01.

Finally, it should be noted that upon excitation at the ligand (270 nm), the solid state photoluminescence spectra of **1** (Figure 6) exhibits two emission bands at 484 nm and 575 nm, respectively, which correspond with the characteristic emission $^4F_{9/2} \rightarrow {}^6H_J$ (J = 15/2, 13/2) transitions of Dy^{3+} ion. The yellow emission intensity of $^4F_{9/2} \rightarrow {}^6H_{13/2}$ transition is much stronger than that of the blue one of $^4F_{9/2} \rightarrow {}^6H_{15/2}$, suggesting that the ligand is suitable for the sensitization of yellow luminescence of Dy^{3+}. The emission spectrum of **1** is identical but much more intense than that observed for the monuclear complex $[Dy(H_2L)(NO_3)_3]$,[13] which could be due to the deprotonation of the ligand and the coordination of the Zn^{2+} ion altering the electronic energy levels of the ligand and improving the energy transfer to the excited level of the Dy^{3+} ion.

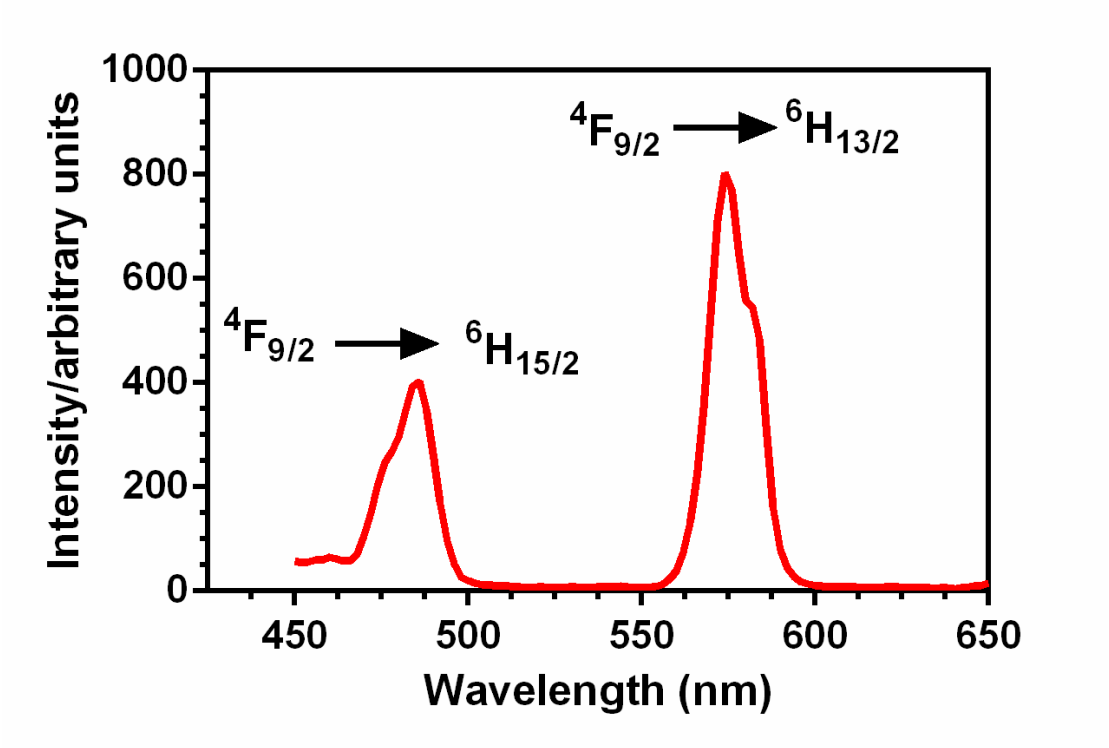

Figure 6. Solid state photoluminescence spectrum of **1**.

Conclusion

We have been able to prepare a tetranuclear Zn_2Dy_2 complex, $\{(\mu_3\text{-}CO_3)_2[Zn(\mu\text{-}L)Dy(NO_3)]_2\}\cdot 4CH_3OH$ from the reaction of the compartmental ligand H_2L (N, N',N"-trimethyl-N,N"-bis(2-hydroxy-3-methoxy-5-methylbenzyl)diethylene triamine) with Zn^{2+} and further with Dy^{3+} in 1: 1 molar ratio and triethylamine. The Zn^{2+} occupies the internal N_2O_3 site whereas the oxophilic Dy^{3+} ion shows preference for the O_4 external site giving rise to the commonly found diphenoxo-bridged ZnDy dinuclear species. In basic medium, carbonate ions are formed form the atmospheric CO_2 and bridge two of these dinuclear units affording the final Zn_2Dy_2 tetranuclear complex. This complex does not show slow relaxation of the magnetization at zero-field due to fast QTM relaxation processes. However, in the presence of a small external dc field, the QTM is partly inhibited and the compound exhibits SMM behavior with an effective thermal barrier U_{eff} = 24 K. Interestingly, the diluted complex crystallized using a 1:10 Dy/Y ratio was shown to almost eliminate the QTM indicating that it occurs by intermolecular dipolar interactions. In this case, SMM behavior is observed at zero field with almost three times higher thermal energy barrier (U_{eff}= 68 K). This is one of the few examples of Dy^{3+} complexes where the SMM behavior is triggered by dilution. The magnetization study of the diluted complex at low temperatures clearly shows that the slow-relaxation of the magnetization is due to the single-ion relaxation of the Dy^{3+}. Even after dilution and in the presence of an applied magnetic field, when the QTM is suppressed (U_{eff}= 78 K), the experimental relaxation times deviate from the Orbach linear law indicating the presence of multiple relaxation processes. It seems that Raman relaxation process significantly affects the Orbach relaxation process reducing the thermal energy barrier U_{eff} for the slow relaxation of the magnetization. Finally, the luminescence spectrum of **1** suggests that the ligand is suitable for the sensitization of yellow luminescence of Dy^{3+}. Therefore, complex **1** can be considered as a bifunctional material exhibiting both SMM behavior and luminescence properties.

We are now pursuing the preparation of new examples of Zn^{2+}-Ln^{3+} complexes with reduced intermolecular interactions that could eventually exhibit suppressed QTM, higher thermal energy barriers at zero-field and therefore improved SMM behavior. Work along this line is currently going on in our labs.

References

[1] Gatteschi, D.; Sessoli R.; Villain J. *Molecular Nanomagnets*. Oxford University Press. Oxford, UK, **2006**.

[2] (a) Aromí, G.; Brechin, E. K. *Struct. Bond*. **2006**, *122*, *1*. (b) Bagai, R.; Christou, G. *Chem. Soc. Rev.* **2009**, *38, 1011*. (c) "Molecular Magnets", themed issue (Editor: E. K. Brechin), *Dalton Trans.* **2010**

[3] (a) Rocha, A. R.; García-Suárez, V.M.; Bailey, S. W.; Lambert, C. J.; Ferrerand, J.; Sanvito, S. *Nat. Mater.* **2005**, *4, 335*. (b) Bogani L.; Wernsdorfer, W. *Nat. Mater*. **2008**, *7, 179.* (c) Affronte, M. *J. Mater. Chem*. **2009**, *19, 1731*.

[4] (a) Leuenberger, M. N.; Loss, D. *Nature*, **2001**, *410, 789*. (b) Ardavan, A.; Rival, O.; Morton, J. J. L.; Blundell, S. J.; Tyryshkin, A. M.; Timco, G. A.; Winpenny, R. E. P. *Phys. Rev. Lett.*, **2007**, *98, 057201*. (c) Stamp, P. C. E.; Gaita-Ariño, A. *J. Mater. Chem*. **2009**, *19, 1718*.

[5] (a) Candini, A.; Klyatskaya, S.; Ruben, M.; Wernsdorfer, W.; Affronte, M. *Nano Lett*. **2011**, *11, 2634*. (b) Vincent, R.; Klyatskaya, S.; Ruben, M.; Wernsdorfer, W.; Balestro, F. *Nature* **2012**, *488, 357*. (c) Ganzhorn, M.; Klyatskaya, S.; Ruben M.; Wernsdorfer, W. *Nature Nanotech*. **2013**, *8, 165*.

[6] Some reviews: (a) Rinehart, J. D.; Long, J. R. *Chem. Sci.* **2011**, *2, 2078*. (b) Sorace, L.; Benelli, C.; Gatteschi, D. *Chem. Soc. Rev*. **2012**, *42, 3278*. (c) Luzon, J.; Sessoli, R. *Dalton Trans*. **2012**, *41, 13556*.

[7] Some references for SMMs containing actinide ions: Rinehart, J. D.; Long, J. R. *J. Am. Chem. Soc.* **2009**, 131, 12558; Rinehart, J. D.; Meihaus, K. R.; Long, J. R. *J. Am. Chem. Soc.* **2010**, 132, 7572. Magnani, N.; Apostolidis, C.; Morgenstern, A.; Colineau, E.; Griveau, J.-C.; Bolvin, H.; Walter, O.; Caciuffo, R. *Angew. Chem., Int. Ed.* **2011**, 50, 1696; Antunes, M. A.; Pereira, L. C. J.; Santos, I. C.; Mazzanti, M.; Marçalo, J.; Almeida, M. *Inorg. Chem.* **2011**, 50, 9915.

[8] (a) Andruh, M.; Costes, J. P.; Diaz C.; Gao, S. *Inorg.Chem.* **2009**, *48*, 3342. (Forum Article). (b) Sessoli, R.; Powell, A. K. *Coord. Chem. Rev.* **2009**, *253*, *2328*. (c) Andruh, M. *Chem. Commun.* **2011**, *47*, *3015*.

[9] Some reviews: (a) Guo, Y. N.; Xu, G. F.; Guo, Y.; Tang, J. *Dalton Trans.* **2011**, *40, 9953*. (b) Habib, F.; Mugeresu, M. *Chem. Soc. Rev.* **2012**, *42, 3278*. (c) Clemente-Juan, J. M.; Coronado, E.; Gaita-Ariño, A. *Chem. Soc. Rev.* **2012**, *41, 7464*.

[10] (a) Hewitt, I. J.; Tang, J.; Madhu, N. T.; Anson, C. E.; Lan, Y.; Luzon, J.; Etienne, M.; Sessoli, R.; Powell, A. K. *Angew. Chem. Int. Ed*. **2010**, *49, 6352*. (b) Blagg, R. J.; Muryn, C. A.; McInnes, E. J. L.; Tuna, F.; Winpenny, R. E. P. *Angew. Chem. Int. Ed.* **2011**, *50, 6530*. (c) Ishikawa, N.; Sugita, M.; Tanaka, N.; Ishikawa, T.; Koshihara, S. Y.; Kaizu, Y. *Inorg. Chem.* **2004**, *43*, *5498*. (d) Takamatsu, S.; Ishikawa, T.; Koshihara, S. Y.; Ishikawa, N. *Inorg. Chem.* **2007**, *46, 7250*.

[11] (a) Rinehart, J. D.; Fang, M.; Evans, W. J.; Long, J. R. *Nature Chem.* **2011**, *3, 538*. (b) Rinehart, J. D.; Fang, M.; Evans, W. J.; Long, J. R. *J. Am. Chem. Soc.* **2011**, *133, 14236*.

[12] Meihaus, K. R.; Rinehart, J. D.; Long, J. R. *Inorg. Chem*., **2011**, *50, 8484*.

[13] Ruiz, J.; Mota, A. J.; Rodríguez-Diéguez, A.; Titos, S.; Herrera, J. M.; Ruiz, E.; Cremades, E.; Costes, J. P.; Colacio, E. *Chem. Commum*. **2012**, *48, 7916*.

[14] (a) Colacio, E.; Ruiz, J.; Mota, A. J.; Palacios, M. A.; Cremades, E.; Ruiz, E.; White, F. J.; Brechin, E. K. *Inorg. Chem.* **2012**, *51, 5857* (b) Colacio, E.; Ruiz, J.; Mota, A. J.; Palacios, M. A.; Ruiz, E.; Cremades, E.; Hänninen, M. M.; Sillanpää, R.; Brechin, E. K. *Comptes Rendus Chimie*, **2012**, *15, 878*.

[15] Watanabe, A.; Yamashita, A.; Nakano, M.; Yamamura, T.; Kajiwara, T. *Chem. Eur. J*. **2011**, *17, 7428*.

[16] Yamashita, A.; Watanabe, A.; Akine, S.; Nabeshima, T.; Nakano, M.; Yamamura, T.; Kajiwara; T. *Angew. Chem. Int. Ed.* **2011**, *50, 4016*.

[17] Altomare, A.; Burla, M.; Camalli, M.; Cascarano, G. L.; Giacovazzo, C.; Guagliardi, A.; Moliterni, A. G. G.; Polidori, G.; Spagna, R. *J. Appl. Crystallogr.,* **1999**, *32, 115*.

[18] Sheldrick, G. M. *Acta Crystallogr. Sect A,* **2008,** *64, 112*.

[19] Farrugia, L. *J. Appl. Cryst*. **1999**, *32, 837*.

[20] Topas-R, Bruker AXS: General profile and structure analysis software for powder diffraction data.

[21] (a) Vallejo, J.; Cano, J.; Castro, I.; Julve, M.; Lloret, F.; Fabelo, O.; Cañadillas-Delgado, L.; Pardo, E. *Chem. Commun*. **2012**, *48, 7726*. (b) Langley, S. K.; Moubaraki, B.; Murray, K. S. *Inorg. Chem.* **2012**, *51, 3947*. c) Sakamoto, S; Fujinari, T.; Nishi, K.; Matsumoto, N.; Mochida, N.; Ishida, T.; Sunatsuki, Y.; Re, N. published in the web, *http:/dx.doi.org/ 101021/ic4008312l.*

[22] Zhang, P.; Zhang, L.; Lin, S. Y.; Tang, J. *Inorg. Chem.* published in the web, *http:/dx.doi.org/ 101021/ic400620j*

[23] Zhang, B.; Zheng, X.; Su, H.; Du, C.; Song, M.; *Dalton Trans.* **2013**, 42, 8571.

[24] Colacio, E.; Ruiz, J.; Lorusso, G.; Brechin, E. K.; Evangelisti, M. manuscript in preparation

[25] Abragam, A.; Bleaney, B. *Electron Paramagnetic Resonance of Transition Ions*, Clarendon Press. Oxford, **1970**.

[26] Shirivastava, K. N. *Phys. Status Solidi B,* **1983**, *117, 437*.

[27] Wernsdorfer, W. *Supercond. Sci. Technol.* **2009**, *22, 064013.*

[28] Wernsdorfer, W.; Chakov, N.E.; Christou, G. *Phys. Rev. B*, **2004**, *70, 132413*.

[29] Guo, Y. N.; Xu, G. F.; Wernsdorfer, W.; Ungur, L.; Gao, Y.; Tang, J.; Zhang, H. J.; Chibotaru, L. F.; Powell, A. K. *J. Am. Chem. Soc*, **2011**, *133, 11948*.